International Symposium
On Turbulence and Shear Flow
Phenomena (TSFP-8)
August 28 - 30, 2013 Poitiers, France

EXPERIMENTAL INVESTIGATION OF STEADY CIRCULATION CONTROL BLOWING OVER A ROUNDED WINGTIP

Adam M. Edstrand
Department of Mechanical Engineering
Florida Center for Advanced Aero-Propulsion, Florida State University
2003 Levy Ave, Tallahassee, FL 32310, United States of America
ae12e@my.fsu.edu

Louis N. Cattafesta III
Department of Mechanical Engineering
Florida Center for Advanced Aero-Propulsion, Florida State University
2003 Levy Ave, Tallahassee, FL 32310, United States of America
lcattafesta@fsu.edu

ABSTRACT

Wingtip vortices are an adverse by-product of lift generation on an airfoil. To study the control of these vortices, a semi-span NACA 0012 airfoil model with a rounded wingtip is mounted in an open-jet wind tunnel. The wake of the vortex is measured from 1.5 to 5.25 chords downstream of the leading edge of the airfoil via stereo particle image velocimetry. Spatially uniform and segmented steady blowing from a chordwise slot on the suction side of the rounded wingtip are used as control. For uniform blowing, there is a peak reduction in the average of the maximum swirl velocity, associated with the wake-hazard problem, by nearly 30%. However, there is a monotonic increase in circulation with increasing momentum coefficient, increasing the strength of the vortex and potentially modifying the lift on the wing. The segmented-steady blowing configuration had minimal effect on circulation for low momentum coefficient values while reducing the maximum of the time-averaged swirl velocity by 20% for a momentum coefficient of 0.0023.

INTRODUCTION

The pressure imbalance on the tip of a finite aspect ratio wing drives a net flow about the wingtip, generating a wingtip vortex that separates and convects downstream. Since vorticity is solenoidal, the vortex persists far downstream of the wing. These vortices induce a downward velocity behind the wing, called downwash, causing induced drag, which is approximately 40% of the drag on a typical aircraft (Kroo, 2001), contributing to a large percentage of the cost of fuel in air travel. These vortices are also the prominent noise source of helicopters in flight due to blade-vortex interaction causing large amounts of noise pollution in urban areas. In addition, the time required for these vortices to decay dictates the timing between successive takeoffs and landings for the safety of following aircraft. Generally these vortices decay or break up by viscous diffusion or the excitation of the Crow instability (Spalart, 1998).

In maritime applications, these vortices are also shed downstream of sails. With the deflection of these sails or a sideslip angle over the sail caused by ocean currents, a wingtip vortex is generated. The Crow instability cannot be leveraged in this instance because two counter rotating vortices are required. Therefore, the breakup of this single vortex is solely due to slow process of viscous diffusion. This persistent vortex leaves a footprint that may be observable, which may be an undesirable attribute for underwater vehicles. Wingtip vortices prove to be resilient to the application of control, and therefore are a popular topic in engineering research.

In an attempt to control these vortices, winglets are often added to the wing as a method of passive control. However, passive control is only optimized for one flight condition and is generally inefficient or ineffective at the other times in flight. Implementing active control allows for various levels of control to address a variety of flight conditions, enabling effective control over the entire flight envelope. The adaptability of active control is useful in this application because the vortex strength is significantly higher during takeoff and landing relative to the strength during cruise.

Recent research in active control of wingtip vortices include two prominent control philosophies. The more frequently implemented technique attempts to accelerate the Crow instability, allowing the two counter-rotating vortices to break up into less hazardous vortex rings (Matalanis & Eaton, 2007; Spalart, 1998). This commonly involves changing the spanwise lift distribution along the wing, while keeping the overall lift constant. This however tends to increase stress levels and fatigue on the structure of the wing. The second philosophy attempts to decay the vortex via cross-diffusion of vorticity. This includes introducing equal and opposite vorticity near the wingtip. Previously studied methods for achieving this use blowing in the wingtip region (Margaris & Gursul, 2010; Mathewson *et al.*, 1998).

In the present work, blowing over a rounded wingtip along the suction side of the airfoil is examined. This

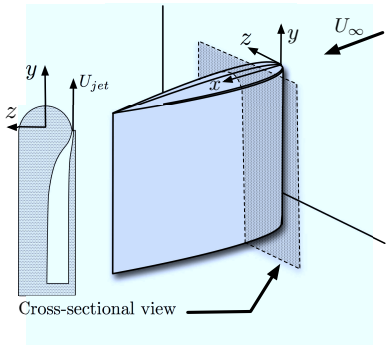

Figure 1. Schematic of the airfoil placed in the test section. Cross-section of airfoil shown to the left. The slot covers the first 75% of the airfoil chord.

method of blowing leverages the Coanda effect, where the blowing over the rounded wingtip wraps around the wingtip, countering the nascent vortex motion. Though the vortex topology of a similar control methodology has been mapped (Margaris & Gursul, 2010), the downstream effect of wingtip blowing has not been investigated. In addition, segmented-chordwise blowing is also investigated. This changes the uniform slot into a periodic blowing slot where the spacing of the segmented blowing is determined by the secondary instability length of flow over a cylinder **??**.

This paper is organized as follows. First, an overview of the experimental setup and methodology is examined. Then the results and discussion of the uniform and segmented blowing cases are presented. Finally, the results and conclusions are discussed, and future work is presented.

SETUP AND METHODOLOGY

A 30.5 cm chord, 38.1 cm half-span NACA 0012 airfoil with a rounded wingtip is placed in the University of Florida Anechoic Flow Facility (UFAFF). The UFAFF is a open-jet wind tunnel placed inside an ISO 3745-certified 100 Hz anechoic chamber (Mathew *et al.*, 2005). The test section is 0.74 m tall by 1.12 m wide by 2.83 m in the flow direction. A schematic of the model, coordinate system, and the wingtip cross-section is shown in Figure 1. The wing is mounted on the floor of an acoustic foam sidewall. All present results are performed at a chord Reynolds number of 530k, corresponding to a test-section speed of 27 m/s, at an angle of attack of 5 degrees.

The air supply for blowing is dried and filtered prior to entering the model at the root of the wing. Plenum temperature and pressure are measured to approximate the flow velocities via the isentropic relation shown in Equation 1. Constant-temperature hot-wire anemometry is used to characterize the flow uniformity across the slot and determine the validity of Equation 1. The flow along the center of the slot proves to be uniform, but the region near the ends has a slight reduction in velocity due to end effects. The nominal jet velocity is predicted by Equation 1 to within experimental uncertainty.

$$U_{jet} = \left[2\frac{\gamma R T_o}{\gamma - 1} \left(1 - \left(\frac{P_\infty}{P_o} \right)^{\frac{\gamma-1}{\gamma}} \right) \right]^{\frac{1}{2}} \qquad (1)$$

The parameter used to quantify blowing is the dimensionless momentum coefficient, shown in Equation 2.

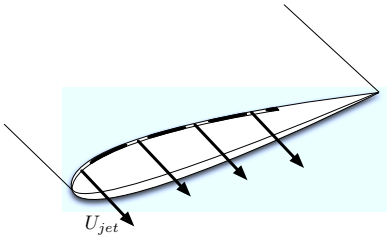

Figure 2. Segmented-chordwise blowing configuration.

$$C_\mu = \frac{\dot{m} U_{jet}}{q_\infty b c} = 2 \left(\frac{U_{jet}}{U_\infty} \right)^2 \frac{A_{slot}}{bc} \qquad (2)$$

where b is the half-span, h is the slot height set at 1 mm, A_{slot} is the cross-sectional area where the jet issues from the slot, and U_{jet} and U_∞ are the jet and free stream velocity, respectively.

Two blowing configurations are studied. The first configuration is uniform blowing from the entire slot, shown in Figure 1. This is performed for momentum coefficients from 0.0021 to 0.0434. The second case involves segmented-chordwise blowing from the slot, shown in Figure 2. The spacing between blowing regions is based on the wavelength of the secondary instability of flow over a cylinder at low Reynolds number. Previous research has found this wavelength to be approximately $\lambda = 4D$, where D is the cylinder diameter (Barkley & Henderson, 1996). Since the diameter of the rounded wingtip varies with position along the chord, the average diameter from 0% to 75% of the airfoil chord is used. This results with a spacing with a wavelength of 0.03 m. This reduces the mass flow rate and thus the momentum coefficient for these cases by 48%. This case is only performed for the blowing cases corresponding to momentum coefficients of 0.0023, 0.0093, and 0.208.

Stereo Particle Image Velocimetry

Measurements in the wake of the wing are made via stereo particle image velocimetry (SPIV). An Evergreen 120 mJ PIV Nd:Yag laser emits a laser that is spread into a 2 mm light sheet for two LaVision Imager Pro X 4M 2048 by 2048 pixel cameras to acquire data. A LaVision portable timing unit synchronizes the camera and laser. The light sheet is positioned between 1.5 and 5.25 chords downstream of the airfoil's leading edge, dictating the range of experimental measurement planes. A TSI 9307-6 oil droplet generator dispenses the nominal 1 μm diameter seed particles (Melling, 1997) into the flow by a custom made seeding system placed downstream of the inlet flow straighteners and turbulence screens.

The image pairs are converted to vector fields via DaVis 8.0 software using a multi-pass approach with a final interrogation window of 32x32 pixels. After the vector fields are calculated, post-processing removes erroneous vectors and further processing is then performed in MATLAB. For fully converged statistics, 500 image pairs are acquired at two downstream chord locations: $x/c = 1.5$ and $x/c = 5.0$. For a broader view of the average flowfield in order to examine the vortex evolution, 50 image pairs are acquired from $x/c = 1.5$ to 5.25 in 0.25 increments. The 50

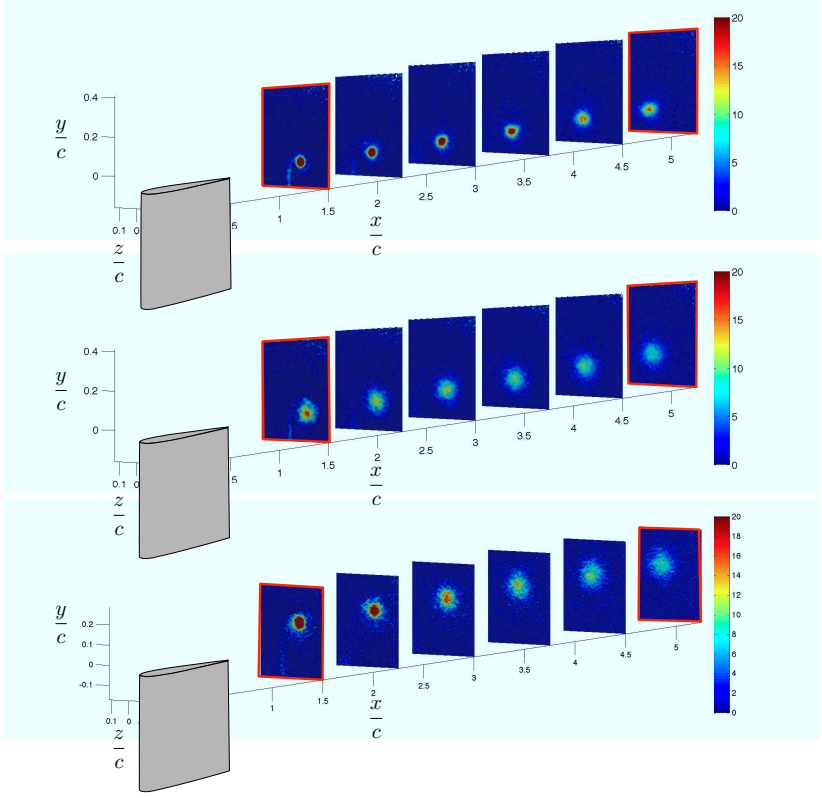

Figure 3. Time-averaged flow topology of the baseline case (top), the low blowing case (middle), and the medium blowing case (bottom). The low and medium blowing cases correspond to uniform steady blowing with a C_μ of 0.0048 and 0.0193, respectively. Contours are normalized vorticity. Red lines indicate the position of converged data measurement planes.

image pairs provide data that are accurate to within 10% of the converged values.

Metrics of Control Effectiveness

Different control objectives require different metrics to determine the effectiveness of control. Circulation is used to determine how the control affects the vortex strength. The three objectives that are investigated are reduction in the wake-hazard problem, the vortex detection problem, and the overall diffusion of average vorticity.

The circulation of the vortex characterizes the vortex strength. The mean circulation, Γ, is the vorticity flux integrated over the measurement plane, shown in Equation 3. The vorticity field is calculated from a second order central-difference method of numerical differentiation of the velocity field. Vortex wandering does not have an effect on the calculated circulation (Devenport *et al.*, 1996). The circulation is normalized by the bound circulation of the airfoil. The bound circulation levels are determined from Prandtl's lifting line theory and are a function of angle of attack and the aspect ratio of the airfoil. Since the airfoil is mounted to the wind tunnel wall, the aspect ratio is reduced by the boundary layer thickness of the sidewall. The height of the boundary layer is subtracted from the span, resulting in an effective span and thus an effective aspect ratio of 2.25.

$$\Gamma = \iint_A \left(\nabla \times \overline{\mathbf{V}}\right) \cdot d\mathbf{A} \tag{3}$$

The maximum of the time-averaged swirl velocity of the flowfield, $\overline{V}_{\theta,max}$, is an indirect measure of the amount of vortex diffusion and can be used as a metric in vortex detection applications. First the velocity field is averaged, and then the maximum swirl velocity is determined, shown in Equation 4.

$$\overline{V}_{\theta,max} = \max\left(E\left[V_\theta\right]\right) \tag{4}$$

The average of the maximum instantaneous swirl velocity, $\hat{V}_{\theta,max}$, addresses the problem of the vortex effect on adjacent aircraft. The maximum swirl velocity is found for each image pair and then averaged over all image pairs to determine the average value, shown in Equation 5. Since the maximum is found for each image pair, wandering does not corrupt the calculation of this quantity.

$$\hat{V}_{\theta,max} = E\left[\max\left(V_{\theta,i}\right)\right] \tag{5}$$

RESULTS AND DISCUSSION

First, the downstream evolution of the vortex for different blowing configurations is addressed, followed by the results and discussion of the uniform chordwise blowing case. Finally, the results of the segmented-chordwise blowing measurements are given and compared with the uniform blowing results.

Vortex Topology and Evolution

Mean vorticity values for multiple locations downstream of the airfoil are shown in Figure 3. In the baseline flow case, shown at the top of Figure 3, a coherent

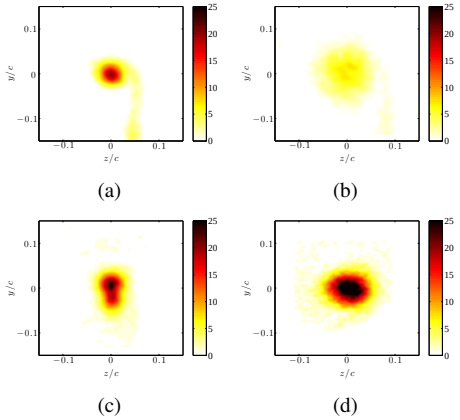

Figure 4. Normalized vorticity contours at 1.5 chords downstream of the leading edge for uniform blowing at a C_μ of (a) 0, (b) 0.0048, (c) 0.0193, and (d) 0.0434.

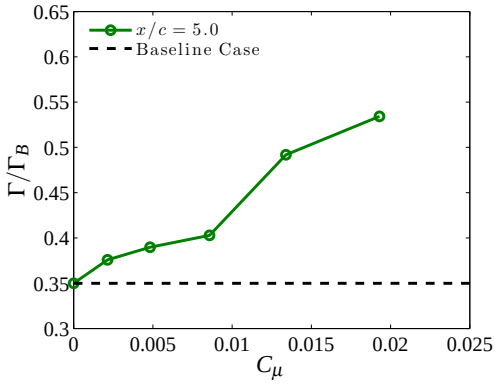

Figure 5. Non-dimensional circulation versus momentum coefficient for uniform blowing. Circulation is normalized by the theoretical bound circulation.

wingtip vortex is clearly present downstream of the airfoil. It diffuses as it convects downstream. This apparent diffusion is largely attributed to larger wandering levels that increase with downstream progression (Devenport *et al.*, 1996). With the application of low blowing control uniformly across the slot ($C_\mu = 0.0048$), shown in the middle image of Figure 3, there is a clear reduction in the coherence of the wingtip vortex, and apparent diffusion increases relative to the baseline case with downstream progression. With a further increase in blowing ($C_\mu = 0.0193$), shown at the bottom of Figure 3, the vortex increases in size and vorticity levels at upstream locations but diffuses rapidly with further downstream progression.

As shown in Figure 3, the vortex is not completely rolled up until 3 to 4 chords downstream of the airfoil's leading edge. This is because at the upstream location the vortex sheet shed from the airfoil is not fully rolled up into the wingtip vortex. Therefore, circulation levels at the downstream location are more pertinent than the upstream location. However, the upstream locations are important for the swirl velocity parameters to determine how the jet interacts with the wingtip vortex.

Uniform Chordwise Blowing

The control jet injects mass and momentum into the flow, interacting with the vortex depending on the prescribed plenum pressure. Figure 4 shows a view of the normalized vorticity contours, $\omega^* = \frac{\omega c}{U_\infty}$, illustrating how different control levels affect the vortex differently at the upstream ($x/c = 1.5$) location. The uncontrolled baseline case, shown in Figure 4(a), has a strong, coherent vortex with the vortex sheet from the wing's wake clearly present. As the momentum coefficient increases to $C_\mu = 0.0048$, shown in Figure 4(b), the vortex core increases with size and the vortex sheet becomes less distinguished and apparent, nearly separating from the main vortex. With medium and high blowing coefficients (*e.g.* $C_\mu = 0.0193$ and 0.0434 for Figures 4(c) and 4(d), respectively), the vortex core is larger with higher vorticity levels relative to the baseline case, signifying an over-actuation of the control resulting in a strengthening of the vortex.

Indeed, the circulation tends to increase with larger C_μ values, shown in Figure 5. From the baseline case, the circulation monotonically increases with increased jet momentum. This may indicate that the control jet may not be attaching to the rounded wingtip due to the Coanda effect as hypothesized. Another possibility is that the control jet acts like a jet in crossflow, and the downstream vorticity from the shear layer bends backwards towards the suction side of the airfoil, adding to the vorticity of the wingtip vortex. After the initial reduction, there is a monotonic increase for both downstream locations. This seems to be indicative that for the vortex detection problem, there is not much improvement in the metric at the downstream location.

Figure 6 shows an initial dip in $\overline{V}_{\theta,max}$ followed by a monotonic increase with increase in C_μ. This indicates that, with respect to the vortex detection problem, there is modest improvement at the upstream location, but not much improvement further downstream. Indeed, $\overline{V}_{\theta,max}$ reduces 25% at the upstream locations, but at the downstream location, there is a less than 10% reduction. However, this should be noted with caution since the swirl velocities in Figure 6 are normalized by the baseline swirl velocity at the corresponding downstream location. Since wandering is present, this reduces the baseline swirl velocity downstream (Devenport *et al.*, 1996) by 40%, increasing the apparent levels of the normalized $\overline{V}_{\theta,max}$ values at this location.

Figure 7 helps confirm this with further investigation of $\hat{V}_{\theta,max}$, which is independent of wandering levels. Similar to the $\overline{V}_{\theta,max}$ case, there is an initial dip, followed by a monotonic increase afterwards. The trends of the upstream and downstream locations are similar in shape with an offset between the two locations. At the downstream location, $\hat{V}_{\theta,max}$ is reduced by nearly 30%, which yields good improvement for the wake vortex problem. The higher levels at the upstream location are attributed to the close proximity of the measurement plane to the jet.

With the qualitative and quantitative effects of the uniform blowing presented, a fair comparison with the segmented-chordwise configuration is possible and examined in the next section.

Segmented-Chordwise Blowing

The use of segmented-chordwise blowing along the slot has the advantage of achieving potentially comparable or better control capabilities with reduced control input, reducing the amount of mass necessary for the control. The simplest modification is blocking specific regions of the slot, allowing for several discrete blowing slots that

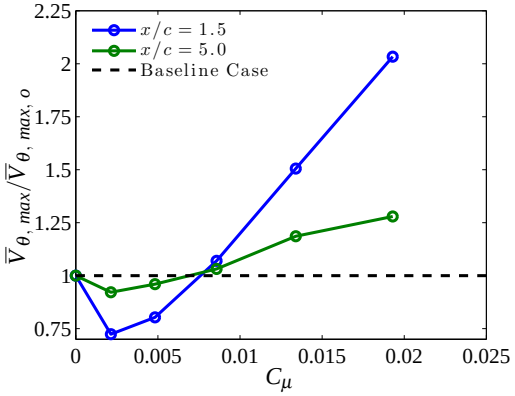

Figure 6. Maximum time-average swirl velocity normalized by the corresponding baseline uncontrolled case versus momentum coefficient for uniform blowing.

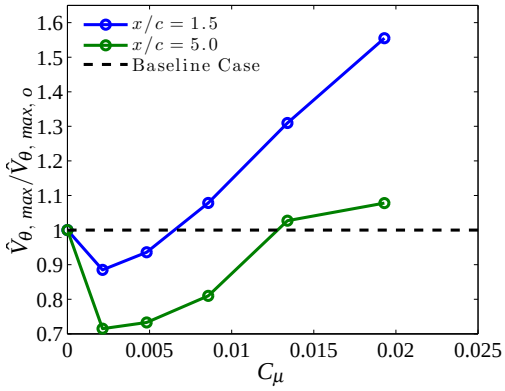

Figure 7. Average of the maximum swirl velocity normalized by the corresponding baseline uncontrolled case versus momentum coefficient for uniform blowing.

reduce the mass flow rate by 48%. For an overview of the effects of different blowing levels, the normalized vorticity contours are shown in Figure 8. Similar to the uniform blowing configuration, the low blowing case, shown in Figure 8(b) increases the size, but decreases the high and coherent vorticity levels in the vortex core of the baseline case. Again, further increasing the blowing to higher values increases the size and vorticity levels of the vortex core, signifying the low blowing case is the optimal case as in the uniform blowing case.

Examining the circulation of the segmented-blowing configuration, shown in Figure 9, a negligible change in circulation for low blowing values ($C_\mu = 0.0023$) is observed, contrary to the uniform blowing configuration, shown in Figure 5. However, the shape of the curves of the two configurations is similar. This seems to imply that the amount of momentum injected into the flowfield is directly related to the circulation levels. However, the change in jet position allows for a potentially constant circulation in the vortex for a given control input. Should the circulation of the vortex be indicative of levels of lift, this may be indicative of a control parameter that would not greatly affect the lift of the wing. However, this needs to be confirmed with direct lift measurements.

Similar to the uniform blowing configuration, the value of $\overline{V}_{\theta,max}$, shown in Figure 10, dips prior to monotonically increasing with increasing C_μ. The maximum decrease is

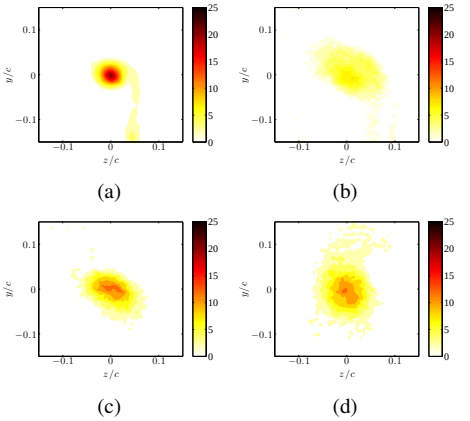

Figure 8. Normalized vorticity contours at 1.5 chords downstream of the leading edge for steady segmented blowing at a C_μ of (a) 0, (b) 0.0025, (c) 0.0010, and (d) 0.0023.

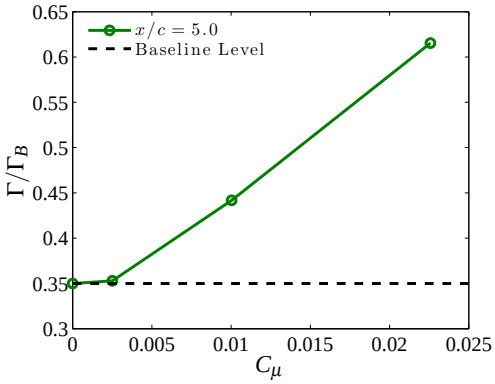

Figure 9. Non-dimensional circulation versus momentum coefficient for steady segmented blowing. Circulation is normalized by the theoretical bound circulation.

nearly 20%, signifying a significant improvement to the vortex detection problem. Contrary to the uniform blowing case, the downstream case is reduced significantly despite the 40% reduction in the baseline swirl velocity caused by wandering. This is a significant improvement over the uniform blowing case shown in Figure 6. This improvement indicates that the distribution of the blowing improves the control effectiveness for the metric associated with the vortex detection problem.

Though there is improvement in $\overline{V}_{\theta,max}$, the segmented-blowing configuration is less beneficial for the wake-hazard metric, $\hat{V}_{\theta,max}$, shown in Figure 11. For the upstream location, there is no improvement for the low blowing case and simply an increase in $\hat{V}_{\theta,max}$. At the downstream location, there is less than a 10% improvement, which implies that the segmented-blowing configuration is less beneficial for the wake-hazard problem than the uniform blowing case, shown in Figure 7.

The variation in the results between the uniform and segmented-blowing configuration indicates that the injected momentum and its distribution largely determine the various metrics. This suggests further research needs to be performed to better understand the reasoning behind these variations in results.

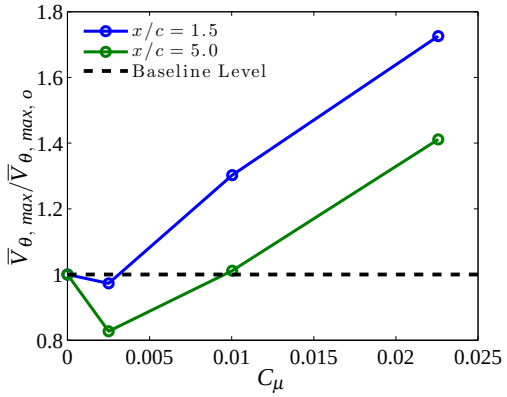

Figure 10. Maximum time-average swirl velocity normalized by the corresponding baseline uncontrolled case versus momentum coefficient for steady segmented blowing.

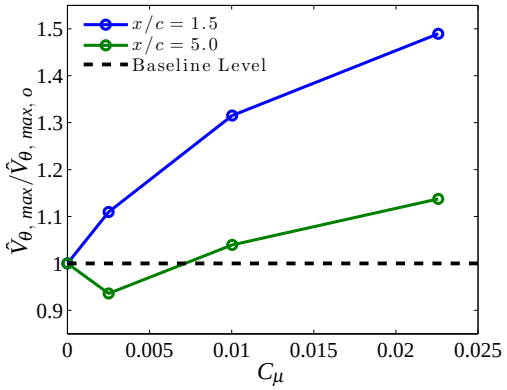

Figure 11. Average of the maximum swirl velocity normalized by the corresponding baseline uncontrolled case versus momentum coefficient for steady segmented blowing.

CONCLUSIONS AND FUTURE WORK

The effects of steady spatially uniform and segmented chordwise blowing on a NACA 0012 wingtip vortex at $Re_c = 530k$ and an angle of attack of 5 degrees have been explored. Changes in three metrics are used to determine the effectiveness of the control: circulation, maximum of the time-averaged swirl velocity, and the average of the maximum instantaneous swirl velocity. A change in circulation is indicative of a modification of vortex strength. A reduction in the maximum of the time-averaged swirl velocity is relevant for vortex detection purposes. Changes in the maximum swirl velocity quantifies the average peak swirl velocity, which is an important metric for the wake-hazard problem.

First, the evolution of the wingtip vortex topology for the baseline and uniform blowing is explored. The results show that for the baseline and control cases, the vortex sheet shed by the wing is not fully rolled up into the vortex until 3 to 4 chords downstream of the leading edge. In general, the low blowing case, corresponding to a momentum coefficient of 0.0048, increases vortex size and reduces the maximum vorticity levels relative to the baseline case for both configurations. For the wake-hazard problem, uniform blowing performs better than segmented blowing, reducing the averaged of the maximum instantaneous swirl velocity levels by nearly 30% compared to 5% for the segmented case. This reduction, however, comes with the cost of adding circulation to the flowfield. On the other hand, for the vortex detection problem, segmented blowing performs better than uniform blowing, reducing the maximum of the time-averaged swirl velocity by nearly 20%, compared to 8% for the uniform case. In addition, the circulation levels at low blowing were not changed drastically for this case, potentially indicating no variation in the lift.

Since the bound circulation ultimately sheds to the vortex, it is important to determine the effect of control on the lift of the airfoil and to quantify the effects of the control on overall drag of the airfoil. Therefore, future measurements of lift and drag via a load cell will be made. In addition, the work in this paper analyzes the effects of blowing downstream of the wing. However, an understanding of the vortex formation process along the surface of the wing may lead to a clearer view of the vortex development and its control. These results would provide insight into how to optimize the control configuration. The differences between uniform blowing and segmented blowing configurations indicate that the momentum and distribution of the control jet greatly influences the control. Future work will thus include an instability analysis with computational studies in an attempt to find an optimal spacing and perhaps frequency.

ACKNOWLEDGEMENTS

This work is supported by NSF PIRE grant OISE-0968313 and the ONR grant N00014-10-1-0832 monitored by Dr. Ronald Joslin.

REFERENCES

Barkley, Dwight & Henderson, Ronald D 1996 Three-dimensional floquet stability analysis of the wake of a circular cylinder. *Journal of Fluid Mechanics* **322**, 215–242.

Devenport, William J, Rife, Michael C, Liapis, Stergios I & Follin, Gordon J 1996 The structure and development of a wing-tip vortex. *Journal of Fluid Mechanics* **312**, 67–106.

Kroo, Ilan 2001 Drag due to lift: concepts for prediction and reduction. *Annual Review of Fluid Mechanics* **33** (1), 587–617.

Margaris, P & Gursul, Ismet 2010 Vortex topology of wing tip blowing. *Aerospace Science and Technology* **14** (3), 143–160.

Matalanis, Claude G & Eaton, John K 2007 Wake vortex control using static segmented gurney flaps. *AIAA journal* **45** (2), 321–328.

Mathew, Jose, Bahr, Chris, Sheplak, Mark, Carroll, Bruce & Cattafesta, Louis N 2005 Characterization of an anechoic wind tunnel facility. ASME.

Mathewson, C. S., Vakili, A. D. & Gowanlock, D. K. 1998 Adaptive control of wingtip vortex flows. In *36th AIAA Aerospace Sciences Meeting and Exhibit, Reno, Nevada*.

Melling, A 1997 Tracer particles and seeding for particle image velocimetry. *Measurement Science and Technology* **8** (12), 1406.

Spalart, Philippe R 1998 Airplane trailing vortices. *Annual Review of Fluid Mechanics* **30** (1), 107–138.